Available online at www.sciencedirect.com

ScienceDirect

Ceramics International 40 (2014) 4267–4276

CERAMICS INTERNATIONAL

www.elsevier.com/locate/ceramint

Camphor sulfonic acid doped polyaniline-tin oxide hybrid nanocomposites: Synthesis, structural, morphological, optical and electrical transport properties

G.D. Khuspe, M.A. Chougule, S.T. Navale, S.A. Pawar, V.B. Patil*

Functional Materials Research Laboratory, School of Physical Sciences, Solapur University, Solapur 413255, MS, India

Received 28 June 2013; received in revised form 21 August 2013; accepted 21 August 2013
Available online 7 September 2013

Abstract

Camphor sulfonic acid (CSA) doped PANi–SnO_2 hybrid nanocomposites were synthesized by solid-state synthesis route with varying amounts (10–50%) of CSA. X-ray diffraction studies have proven the successful incorporation of CSA into the polyaniline–SnO_2 hybrid nanocomposites and the results are also supported by microstructural analysis. UV–visible and Fourier infrared spectroscopy studies have provided insight into the electronic interaction between the CSA, polyaniline, and SnO_2. The room temperature dc electrical conductivity of CSA-doped PANi–SnO_2 hybrid nanocomposite films were observed to depend on the amount of CSA doping and the morphology.

Keywords: C. Electrical properties; C. Optical properties; PANi–SnO_2 hybrid composites; Structural properties

1. Introduction

In recent years, conducting polymers such as polyaniline, polythiophene and polypyrrole have received much attention because of their potential applications in chemical and biological sensors, electronic devices, as well as efficient and low cost solar cells, due to their remarkable mechanical and electrical properties such as low operating temperature, low cost, flexibility and easy processability and so on [1–7]. However, there are also some disadvantages such as low chemical stability and mechanical strength that are unfavorable for conducting polymer-related applications.

Metal oxides can adopt a large variety of structural geometries with an electronic structure that may exhibit metallic, semiconductor, or insulator characteristics, endowing them with diverse chemical and physical properties. Therefore, metal oxides are the most important functional materials used for chemical and biological sensing and transduction. Moreover, their unique and tunable physical properties have made themselves excellent candidates for electronic and optoelectronic applications. Nanostructured metal oxides have been actively studied due to both scientific interests and potential applications [8–13].

Polyaniline is one of the many interesting conducting polymers used in gas sensing, solar cells and supercapacitors [1–7]. Polyaniline can exist in three different oxidation states and the intrinsic redox reactions it can undergo, results in different electrical properties that vary easily with doping, making it suitable for gas sensing application [1–7]. However, an important drawback with polyaniline is its limited mechanical strength. Doping of polyaniline with various acids influences the optoelectronic properties by changing the chemical/structural nature of the polymer and also creating more active sites [14,15]. Potential dopants for polyaniline include camphor sulfonic acid, *p*-toulene sulfonic acid, hydrochloric acid, sulfuric acid, tannin sulfonic acid, lignin sulfonic acid, etc. Among these different dopants camphor sulfonic acid doped polyaniline have enhanced chemical stability and thermal degradation properties and have performed as better anti corrosion materials than polyaniline itself [16,17].

Organic–inorganic (conducting polymer–metal oxide) hybrid materials are currently of great interest for exploring enhanced sensor characteristics, due to their synergetic or complementary behaviors that is not available from their single counterparts [18,19]. The syntheses of PANi–SnO_2 hybrid

*Corresponding author. Tel.: +91 2172744771x202.
E-mail address: drvbpatil@gmail.com (V.B. Patil).

0272-8842/$ - see front matter © 2013 Elsevier Ltd and Techna Group S.r.l. All rights reserved.
http://dx.doi.org/10.1016/j.ceramint.2013.08.091

nanocomposite with different combinations of the two materials have attracted more and more attention, since they have interesting physical properties and potential applications. These particles not only combine the advantageous properties of SnO_2 and PANi, but also exhibit many new characteristics that single-phase materials do not have.

In this article, we report the preparation of CSA-doped PANi–SnO_2 hybrid nanocomposites films by spin coating technique and effect of CSA doping on their structural, morphological, optical and electrical transport properties.

2. Experimental methods

2.1. Materials

Aniline, ammonium peroxydisulfate ($(NH_4)_2S_2O_8$, APS), ammonia (30%), methanol, hydrochloric acid (34%) of analytical reagent grade were used as received from Sd Fine Chem. Ltd., Mumbai. Stannic chloride pentahydrate (Thomas Baker) was used as received and camphor sulfonic acid of 99.9% purity was purchased from Sigma-Aldrich chemicals.

2.2. Preparation of PANi–SnO_2 nanocomposites

PANi–SnO_2 hybrid nanocomposite was prepared by solid-state synthesis route. The details of the synthetic procedure have been published elsewhere [20,21].

2.3. Preparation of CSA-doped PANi–SnO_2 hybrid nanocomposites

Camphor sulfonic acid (CSA) doped polyaniline–SnO_2 hybrid nanocomposites were prepared by adding CSA (10–50%) into polyaniline–SnO_2 nanocomposite matrix. For thin film formation, CSA doped PANi–SnO_2 hybrid nanocomposites were dissolved in m-cresol and stirred for 11 h. Thin films of the CSA doped PANi–SnO_2 hybrid nanocomposites were prepared on glass substrate by using spin coating technique at 3000 rpm for 40 s. and dried on hot plate at 100 °C for 10 min. Fig. 1 shows the flow diagram of synthesis and deposition of CSA doped PANi–SnO_2 hybrid nanocomposites.

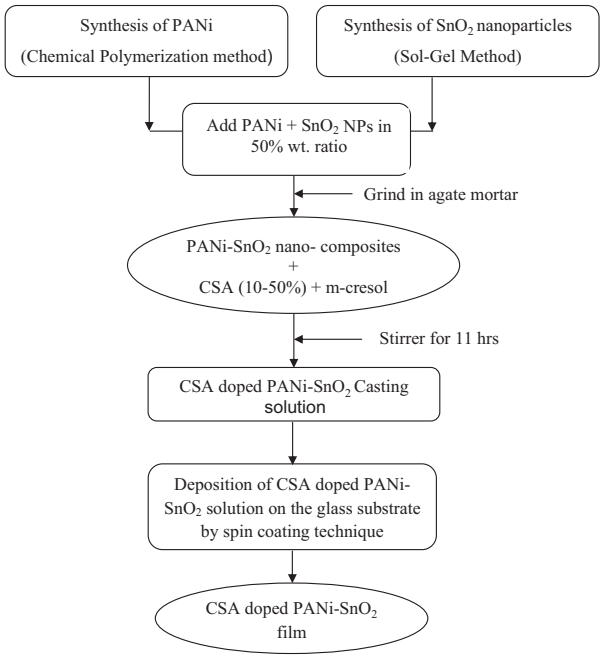

Fig. 1. Flow diagram of synthesis and deposition of CSA doped PANi–SnO_2 hybrid nanocomposites.

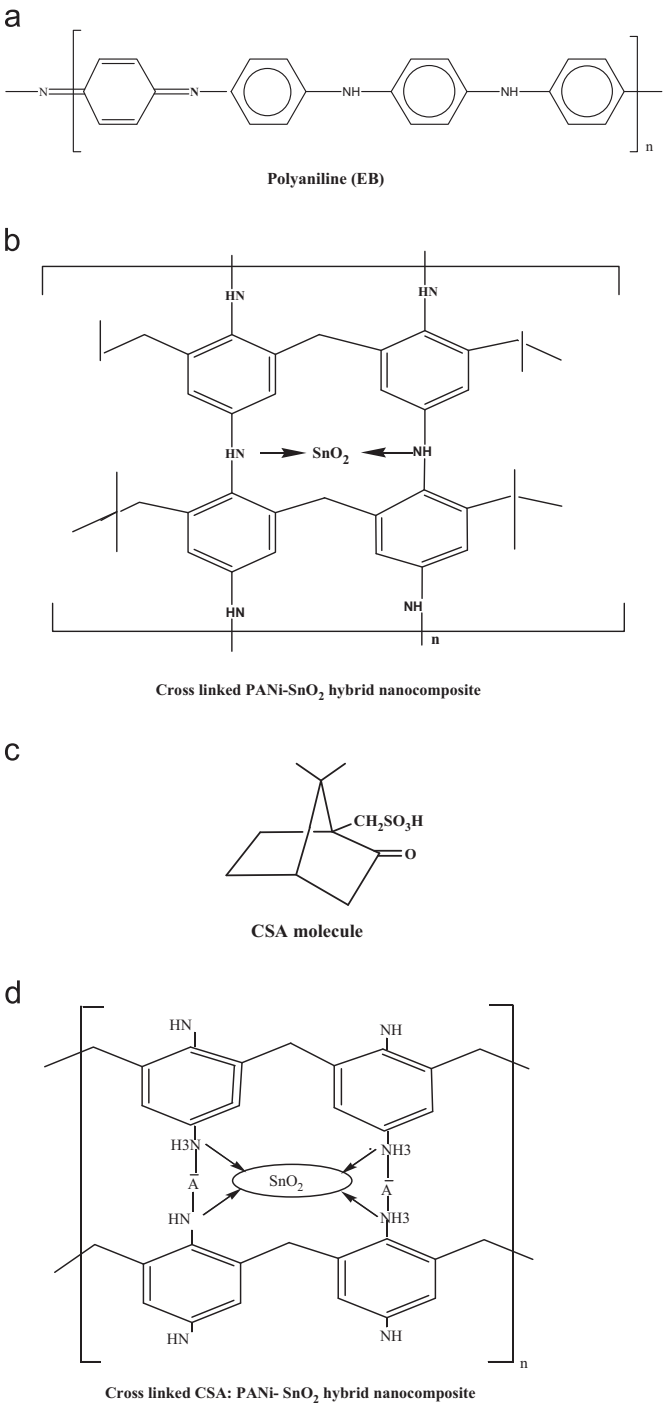

Scheme 1. Reaction mechanism of CSA doped PANi–SnO_2 hybrid nanocomposites; (a) formation of PANi (EB), (b) formation of PANi–SnO_2 hybrid nanocomposite, (c) molecular structure of CSA and (d) formation of CSA doped PANi–SnO_2 hybrid nanocomposite.

2.4. Characterization techniques

The physico-chemical properties of the CSA doped PANi–SnO_2 hybrid nanocomposites were carried out using X-ray diffraction (Model: Philips PW1710 diffractometer (Holland) with CuK_α radiation at step width 0.02°, step time 1.25 s, and $K_\alpha = 1.5406$ Å), fourier transform infrared (FTIR) spectroscopy (Model: Perkin-Elmer 100 spectrophotometer, Santa Clara, CA, USA), field emission scanning electron microscopy (FESEM Model: MIRA3 TESCAN, USA operating at 20 kV), UV–visible spectra of the samples (Model: Simandzu-100 UV–visible spectrophotometer, Kyoto, Japan) were carried out. Roughness of the films were determined using atomic force microscopy (AFM) using AFM, SPA 300 HV. For conductivity measurement, two electrodes, separated by 10 mm, were deposited on CSA-doped PANi–SnO_2 film using silver paint. The room temperature dc electrical conductivity CSA doped PANi–SnO_2 hybrid nanocomposites were measured using custom-made two probe technique. Thickness of polymer hybrid nanocomposites was measured by using AMBIOS-XP1 surface profiler. The obtained values are in the range of 1.10 μm (10% CSA) to 0.92 μm (50% CSA).

3. Results and discussion

3.1. Reaction mechanism of CSA doped PANi–SnO_2 hybrid nanocomposites

Polyaniline (EB) formed by the chemical polymerization method [4,5]. Polyaniline–SnO_2 hybrid nanocomposites formed by adding SnO_2 nanoparticles in the PANi (EB) matrix [20,21]. CSA was added by weight percentage in PANi–SnO_2 hybrid nanocomposites. The possible reaction mechanism for formation of CSA doped polyaniline–SnO_2 hybrid nanocomposites are given in Scheme 1.

3.2. X-ray diffraction (XRD) analysis

Fig. 2 shows the XRD patterns of the PANi (EB), PANi–SnO_2 (50%) and CSA doped (10–50%) PANi–SnO_2 hybrid nanocomposites. The spectra showed sharp and well defined diffraction peaks, indicating the crystallinity of CSA doped PANi–SnO_2 hybrid nanocomposites. Fig. 2(a) shows, the peak at $2\theta = 25–30^\circ$ corresponds to PANi (EB) [4,5]. Other observed 2θ values are consistent with the standard JCPDS

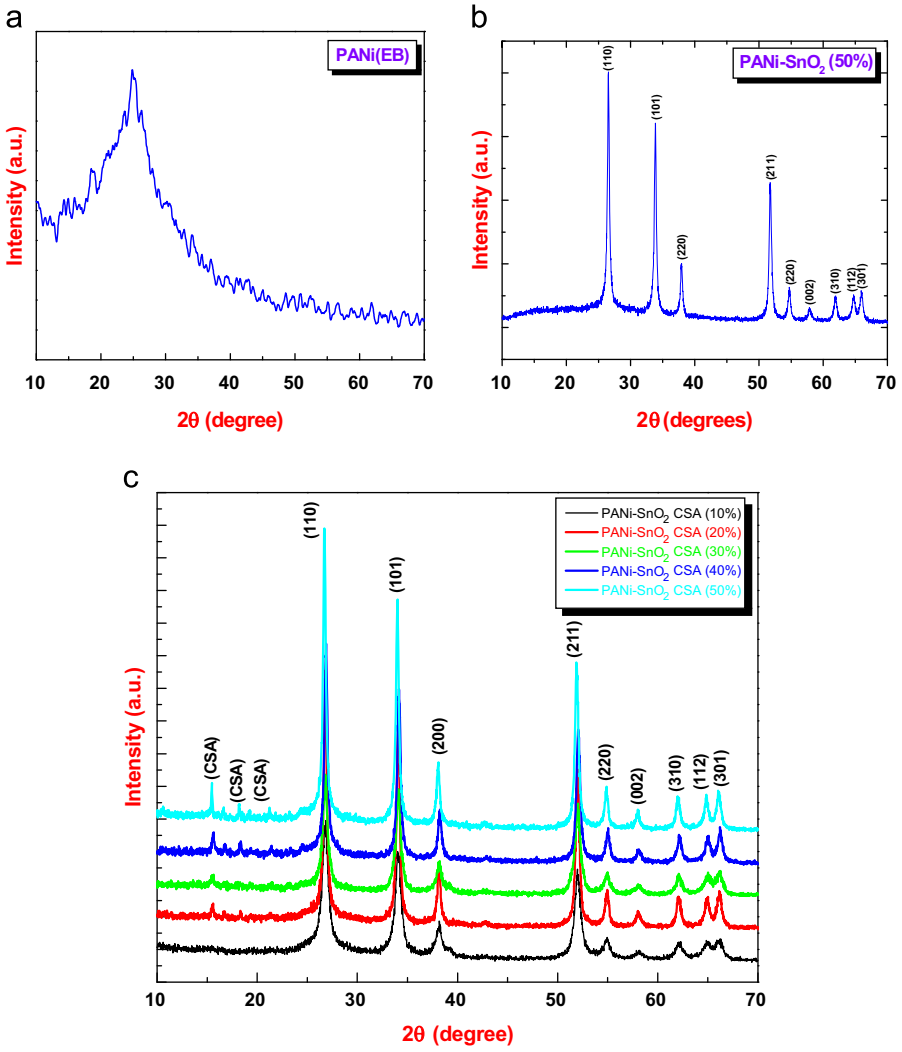

Fig. 2. X-ray diffraction pattern of (a) PANi (EB), (b) PANi–SnO_2 (50%) and (c) CSA doped PANi–SnO_2 (10–50%) hybrid nanocomposites.

values of tetragonal structure of SnO_2 (JCPD File no. 79-0208) [Fig. 2(b)] [22,23]. However, as shown in Fig. 2(c) the peaks at $2\theta = 15.43^\circ$, 16.66°, 18.17°, 19.26° and 21.20° in the crystal pattern of PANi–SnO_2: CSA belong to CSA and their strength is found to be increasing with increasing amount of CSA in PANi–SnO_2 nanocomposites [24]. They are more significant in the 40 wt% and 50 wt% CSA doping patterns. These results indicate the effect of camphor sulfonic acid doping on structural properties of PANi–SnO_2 hybrid nanocomposites.

3.3. Fourier transform infrared spectroscopy (FTIR) analysis

The FT-IR spectrum of the PANi (EB), PANi–SnO_2 (50%) and CSA doped PANi–SnO_2 (10–50%) hybrid nanocomposite in the range 500–4000 cm^{-1} is shown in Fig. 3. For PANi (EB) primly nine absorption peaks are observed [Fig. 3(a)]. The broad band at 3428 cm^{-1} is assigned to the free N–H stretching vibrations of secondary amines [20]. The smaller one peak at 2921 cm^{-1} is characterized to the vibration associated with the NH^{2+} part in the $-C_6H_4NH^{2+}C_6H_4$-group [21,22]. The band at 1559 cm^{-1} is due to quinoid ring deformations of aromatic ring. The peaks at 1470 cm^{-1} and 1292 cm^{-1} are the results of the stretching vibrations of $C–N^+$ and C–N, respectively [23]. The peaks at 1121 cm^{-1} and 801 cm^{-1} are attributed to the aromatic C–H bending in the plane and out of the plane for the 1,4-disubstituted aromatic ring [24,25]. The band at 499 cm^{-1} is attributed to S–C stretching vibration mode, indicating the presence of the chloro group which supports formation of emeraldine PANi hydrogen chloride. Chloronate groups interact with protonated imine nitrogen in neighboring chains and stabilize the PANi. All the above observed absorption characteristics confirm the formation of PANi. The PANi–SnO_2 (50%) hybrid nanocomposites also show [Fig. 3(b)] the same characteristic peaks. However, the corresponding peaks of pure PANi (EB) at 1559 cm^{-1} shifted to 1560 cm^{-1}, 1470 cm^{-1} shifted to 1481 cm^{-1}, 1292 cm^{-1} shifted to 1299 cm^{-1}, 1121 cm^{-1} shifted to 1141cm^{-1}, 801 cm^{-1} shifted to 811 cm^{-1} and 499 cm^{-1} shifted to 504 cm^{-1} wave numbers in PANi–SnO_2 (50%) hybrid nanocomposites. The shift may be ascribed to the formation of hydrogen bonding between SnO_2 and NH group of PANi (EB) on the surface of the SnO_2 particles [26,27]. Fig. 3(c) shows FTIR spectra of PANi–SnO_2: CSA (10–50%). The presence of characteristic IR absorption due to quinoid and benzenoid rings at 1470 cm^{-1} and 1559 cm^{-1}

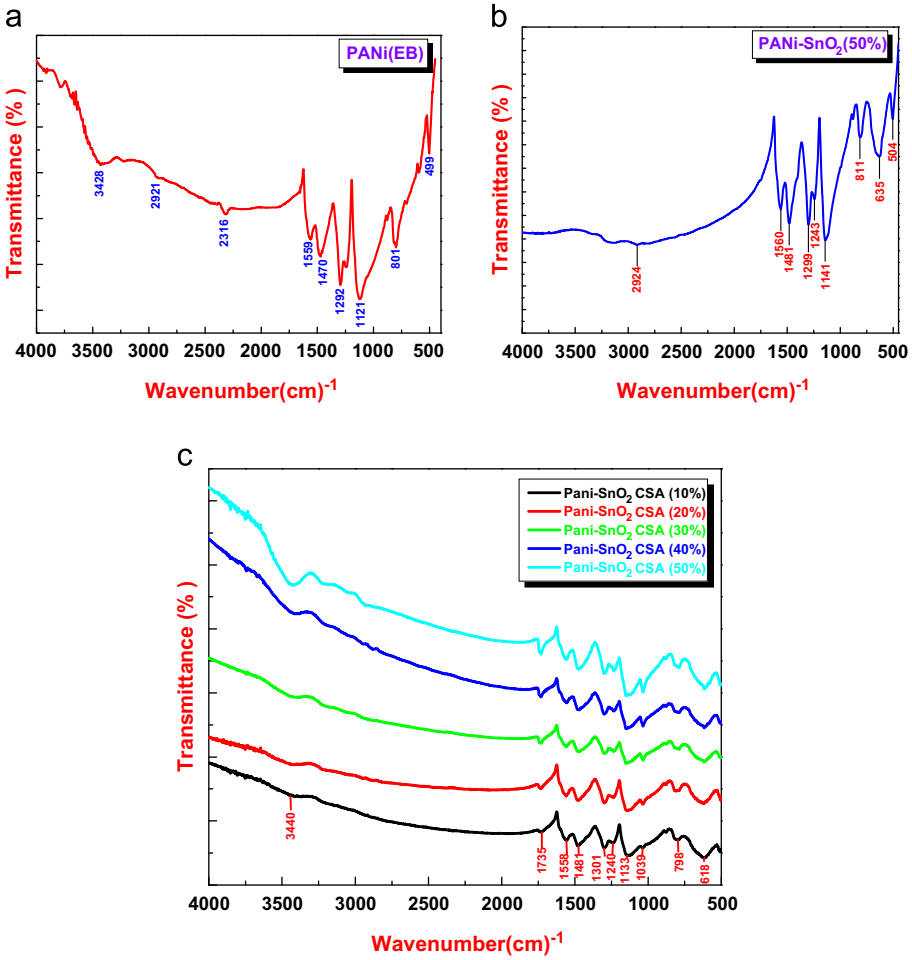

Fig. 3. FTIR spectra of (a) PANi (EB), (b) PANi–SnO_2 (50%) and (c) CSA doped PANi–SnO_2 (10–50%) hybrid nanocomposites.

clearly indicates the two states in the polymer chain. However the red shift in the band is observed from 1470 cm^{-1} to 1481 cm^{-1}. The broad band at 3440 cm^{-1} is due to N–H stretching of aromatic amines. The blue shift of SnO_2 stretching is observed from 811 cm^{-1} to 798 cm^{-1} [28]. This red shift or blue shift can be attributed to the interaction of CSA with PANi–SnO_2 hybrid composites. The presence of CSA is confirmed by the bands at 1039 cm^{-1} (SO^{3-}) and 1735 cm^{-1} (C═O) [29]. The fact that the polymer is the protonated in the part by surface anions is demonstrated by the presence of the peak at 618 cm^{-1}, which is attributed to a stretching vibration in the surface anion [30].

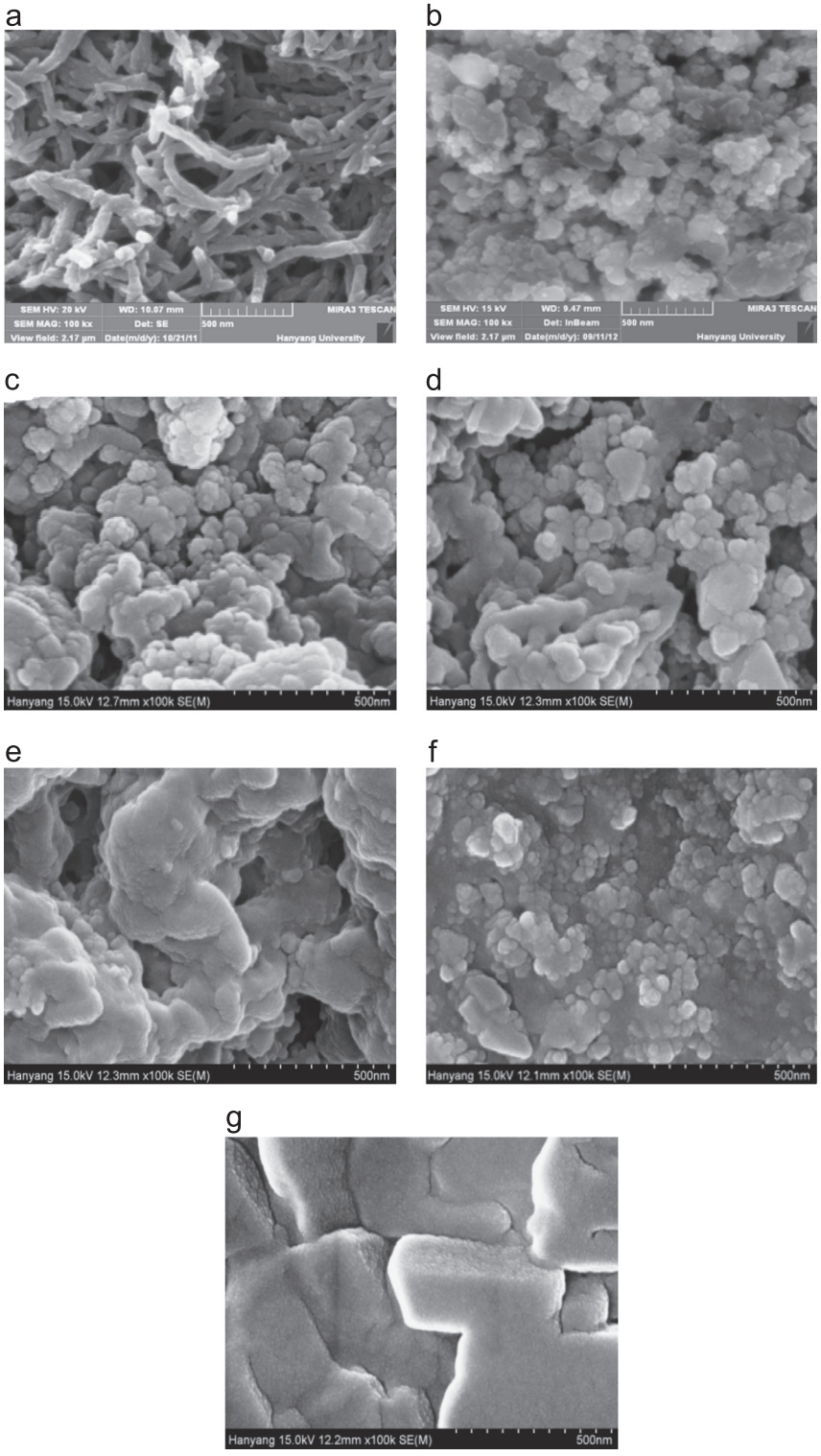

Fig. 4. FESEM of (a) PANi (EB), (b) PANi–SnO_2 (50%) and (c–g) CSA doped PANi–SnO_2 (10–50%) hybrid nanocomposites.

3.4. Field emission scanning electron microscopy (FESEM) analysis

Fig. 4(a)–(c) shows the field emission scanning electron micrographs (FESEM) of PANi (EB), PANi–SnO_2 (50%) and PANi–SnO_2–CSA (10–50%) hybrid nanocomposite films. Fussy nanofibrous morphology of PANi (EB) is as shown in Fig. 4(a). Fig. 4(b) shows the FESEM of a PANi–SnO_2 (50%) nanocomposite film. It shows that the SnO_2 nanoparticles are uniformly distributed into the fibrous PANi matrix, which confirms that the SnO_2 NPs are interacted with PANi. The FESEM micrograph of CSA (10–50 wt%) doped with PANi–SnO_2 (50%) nanocomposite are shown in Fig. 4(c–g). The change in the surface morphology is observed with increasing content of CSA into the PANi–SnO_2 nanocomposite. At lower content of CSA ($\leq 30\%$), the uniform granular dense interconnected morphology attributed to the homogeneous dispersion of CSA into the PANi–SnO_2 nanocomposite. At higher content of CSA ($> 30\%$), porous granular morphology accumulates with voids are observed. Similar change in morphology due to addition of CSA into polymer based hybrid composites were observed by Raut etal and Patil S.L et al. [16,17].

3.5. Transmission electron microscopy (TEM) analysis

Fig. 5 shows the TEM images of the pure PANi (EB), PANi–SnO_2 (50%) and CSA doped PANi–SnO_2 (30%) hybrid nanocomposites. Fig. 5(a) shows the interconnected nanofibrous network of PANi with an average diameter of 36 nm. After the formation of hybrid nanocomposite of PANi–SnO_2 [Fig. 5(b)], the nano-SnO_2 particles (dark shaded nanoparticles) are found to be entrapped into fibrous PANi (light shaded) matrix. This means that the nano-SnO_2 particles are not only simply mixed up or blended with polymer, which is similar to the earlier reports about PANi/nano-SnO_2 composites synthesized by the sol–gel and microemulsion polymerization methods [31,32]. The well-dispersed PANi–SnO_2 (50%) nanohybrid with a diameter of 26 nm are fully wrapped with a thin layer of dopant CSA is shown in Fig. 5(c).

3.6. Atomic force microscopy analysis

The two-(2D) and three-(3D) dimensional surface topology of the PANi, PANi–SnO_2 and CSA doped PANi–SnO_2 thin films were investigated using atomic force microscopy (AFM).

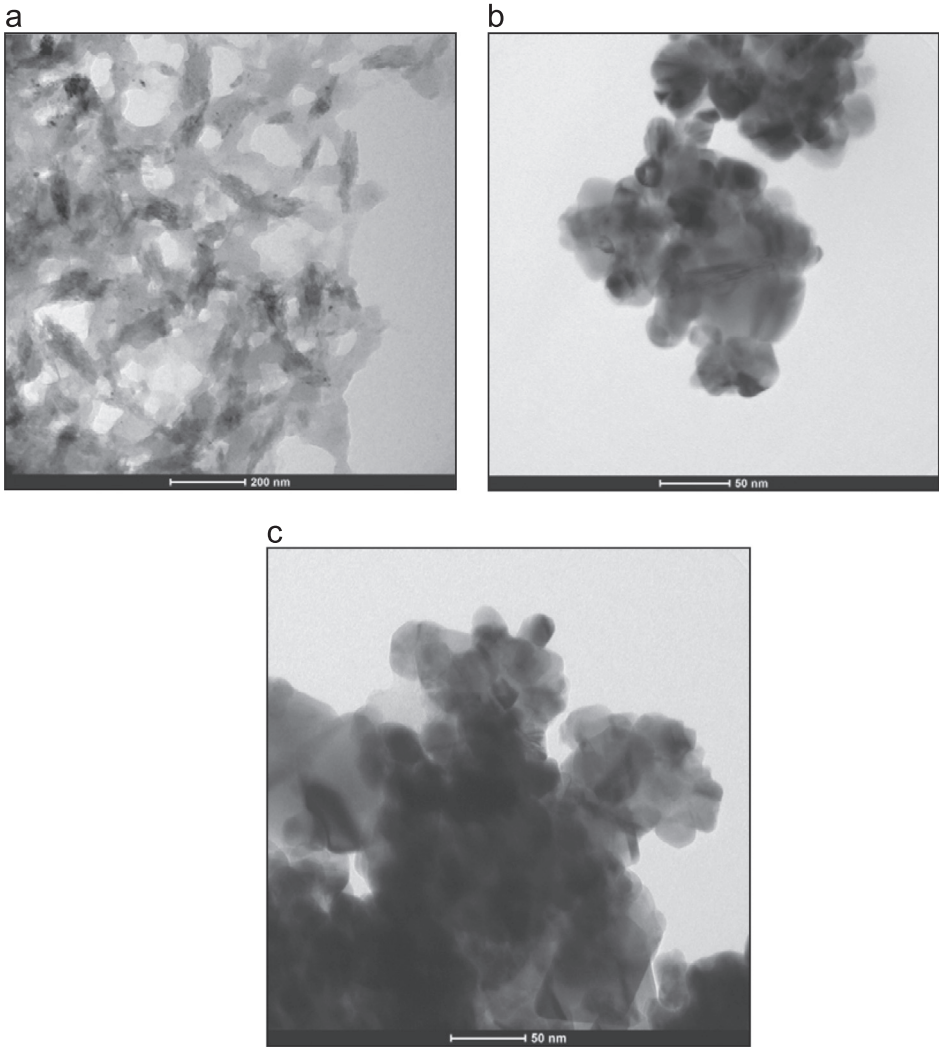

Fig. 5. Transmission electron micrograph of (a) PANi, (b) PANi–SnO_2 (50%) and (c) CSA doped PANi–SnO_2 (30%) hybrid nanocomposites.

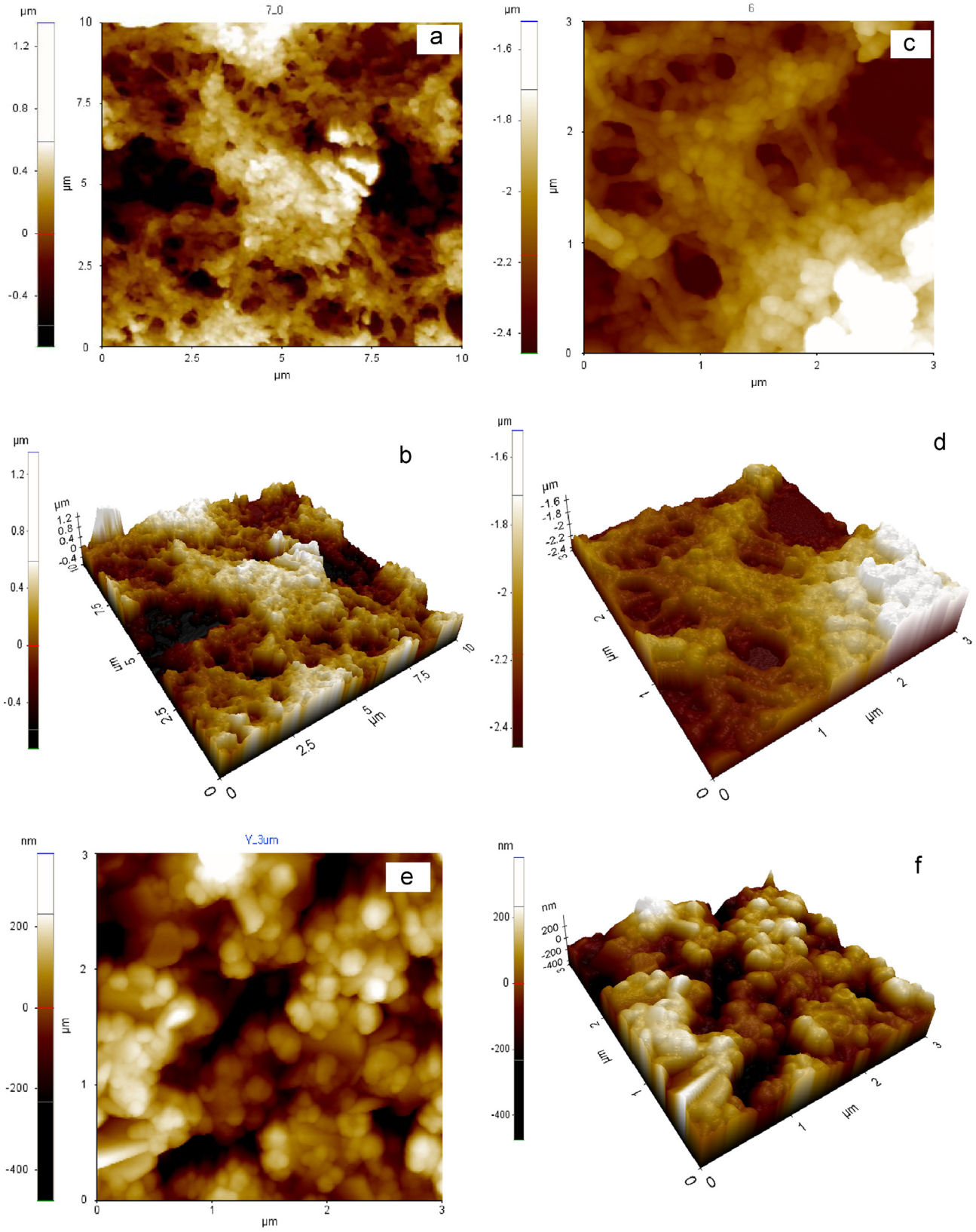

Fig. 6. Atomic force micrograph of (a) 2D PANi (EB), (b) 3D PANi (EB), (c) 2D PANi–SnO_2 hybrid composite, (d) 3D PANi–SnO_2 hybrid composite, (e) 2D CSA (30%): PANi–SnO_2 hybrid composite, and (f) 3D CSA (30%): PANi–SnO_2 hybrid composite.

Fig. 6(a)–(c) shows the 2D and 3D AFM micrographs of PANi (EB), PANi–SnO_2 and 30% CSA doped PANi–SnO_2 hybrid thin films. The PANi image shows micro-porous morphology with average surface roughness 25 nm [4,5]. From the 3D micrograph, it is seen that the film consists interconnected fibers with some visible voids, which is consistent with

FESEM image. The PANi–SnO_2 nanocomposite [Fig. 6(c) and (d)] shows that SnO_2 nanoparticles are composed with PANi. The RMS surface roughness was found to be 31.5 nm for PANi–SnO_2 nanocomposites, which is in between pure PANi and SnO_2 nanoparticles, indicates that the surface of PANi–SnO_2 nanocomposite is smooth. Fig. 6(e) and (f) shows the 2D and 3D topography of CSA doped PANi–SnO_2 hybrid nanocomposites. It shows that the CSA is fully covered by PANi–SnO_2 hybrid nanocomposites.

3.7. UV–visible spectroscopy analysis

Fig. 7 shows the UV–visible absorption spectra of PANi (EB), PANi–SnO_2 and CSA doped PANi–SnO_2 nanocomposites. The PANi shows [Fig. 7(a)] absorption peak at 441 nm can be attributed to the polaron–π* transition [4,5,31]. The peak at 441 nm is due to the protonated form of PANi (EB) [4,5,31]. In the PANi–SnO_2 (50%) hybrid nanocomposites [Fig. 7(b)], the absorption peak of PANi (EB) at 441 nm is shifted to 380 nm. In our previous report, SnO_2 shows a broad range of absorption from 260 nm to 330 nm [22]. By addition of CSA by 30 wt% into the PANi–SnO_2 (50%) hybrid nanocomposites the peak is observed at 378 nm, which is are resulted from following reasons: (1) SnO_2 has the tendency to form the coordination compound with nitrogen atoms in PANi and (2) the hydrogen bonding between PANi and nano-SnO_2.

3.8. Electrical conductivity analysis

Fig. 8 shows the variation of dc electrical conductivity ($\log \sigma$) with increasing doping concentration of CSA into PANi–SnO_2 nanocomposites at the 300 K temperature range. The variation of conductivity over this temperature range clearly shows that the CSA doped PANi–SnO_2 nanocomposites are thermally stable. It is observed that the room temperature conductivity of PANi–SnO_2 nanocomposites increases from 5.98×10^{-9} to 7.28×10^{-8} S/cm as doping concentration of CSA increased from 10% to 50%. This may be attributed to the doping of CSA which maximizes the number of carriers. The highest number of carriers can be connected with the delocalization effect of doping process and formation of the polarons or bipolarons in the composite structure, thus enhancing the conductivity of composite [33–35].

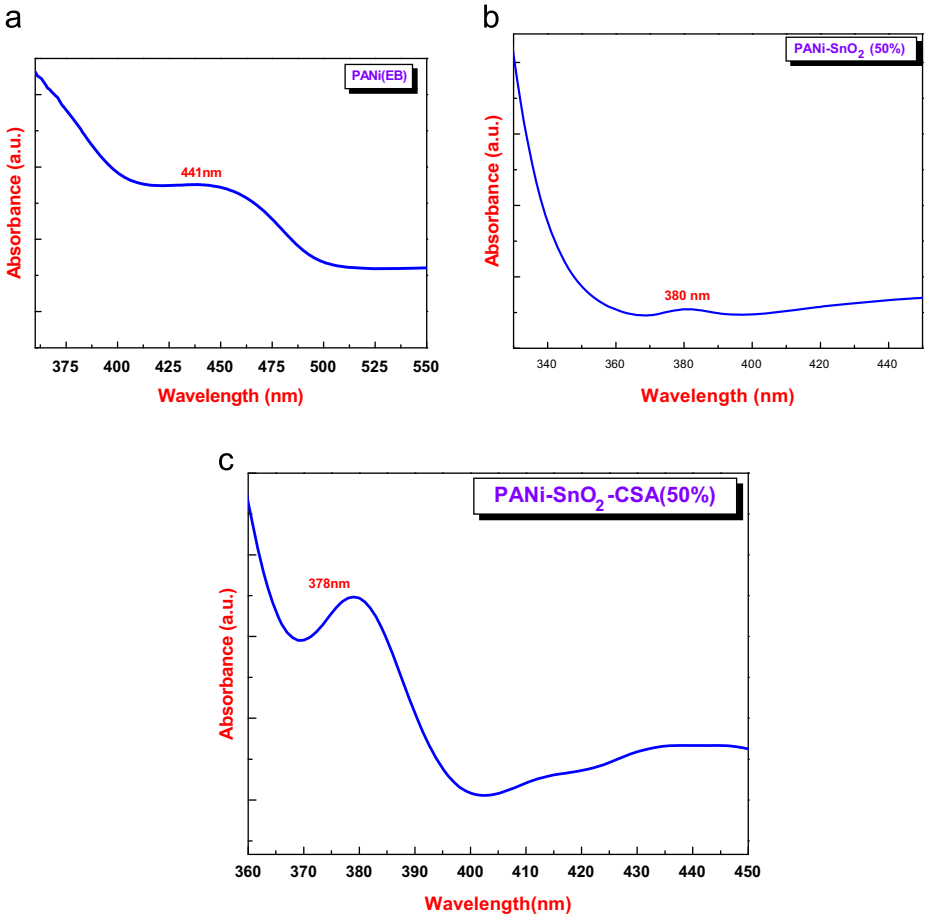

Fig. 7. UV–visible spectra of (a) PANi, (b) PANi–SnO_2 (50%) and (c) CSA doped PANi–SnO_2 (30%) hybrid nanocomposites.

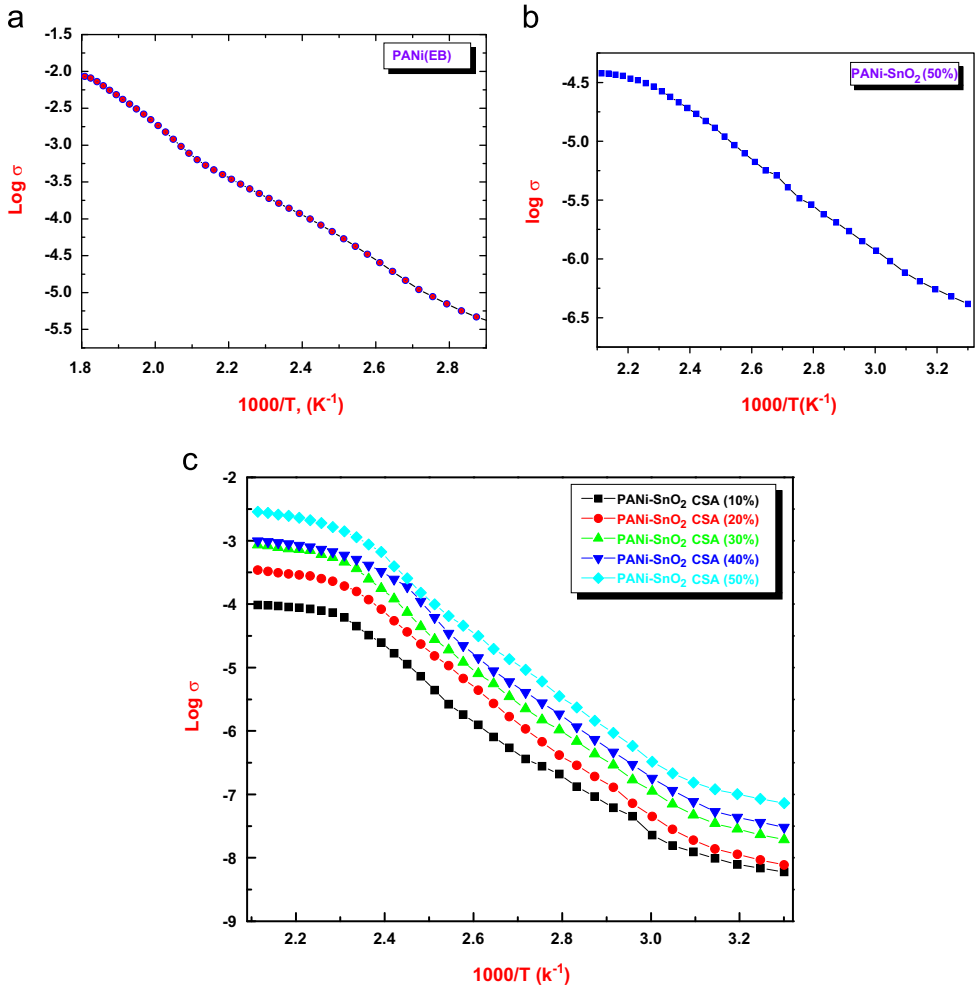

Fig. 8. Electrical conductivity of (a) PANi, (b) PANi–SnO_2 (50%) and (c) CSA doped PANi–SnO_2 (10–50%) hybrid nanocomposites.

4. Conclusion

The CSA doped PANi–SnO_2 hybrid nanocomposite films were successively prepared by spin coating technique on glass substrates. The effect of CSA doping on structural, morphological, electrical transport and optical properties of CSA doped PANi–SnO_2 nanocomposites were investigated by XRD, FTIR, FESEM, UV–visible and two probe techniques. The morphological studies (FESEM) show uniform granular porous morphology of 30% CSA doped PANi–SnO_2 hybrid nanocomposite. From FTIR spectra, it is revealed that the characteristic absorption peaks of PANi–SnO_2 nanocomposite shifted by significant amount into CSA doped PANi–SnO_2 hybrid composite, which indicates that the different interfacial interactions between the CSA and PANi–SnO_2 nanocomposite. The UV spectra shows the absorption peak of PANi–SnO_2 nanocomposite shifts due to addition of CSA confirmed the interaction between CSA and PANi–SnO_2 nanocomposites. The dc electrical conductivity increases with increasing amount of CSA from 10% to 50% into PANi–SnO_2 nanocomposites.

Acknowledgments

The authors (VBP) are grateful to DAE-BRNS, for financial support through the Scheme no. 2010/37P/45/BRNS/1442.

References

[1] B. Adhikari, S. Majumdar, Polymers in sensor applications, Progress in Polymer Science 29 (2004) 699–766.
[2] M.A. Chougule, S.L. Patil, S.G. Pawar, B.T. Raut, P.R. Godse, Shashwati Sen, V.B. Patil, Facile and efficient route for preparation of polypyrrole-ZnO nanocomposites: microstructural, optical and charge transport properties, Journal of Applied Polymer Science 125 (2012) 1418–1424.
[3] M. Woodson, J. Liu, Guided growth of nanoscale conducting polymer structures on surface-functionalized nanopatterns, Journal of the American Chemical Society 128 (2006) 3760–3763.
[4] D.K. Bandgar, D.M. Jundale, G.D. Kuspe, V.B. Patil, Facile and novel route for preparation of nanostructured polyaniline (PANi) thin films, Journal of Applied Nanoscience (2013), http://dx.doi.org/10.1007/s13204-012-0175-8.
[5] G.D. Khuspe, D.K. Bandgar, Shashwati Sen, V.B. Patil, Fussy nanofibrous network of polyaniline (PANi) for NH_3 detection, Synthetic Metals 162 (2012) 1822–1827.

[6] Q.H. Li, J.H. Wu, Q.W. Tang, Z. Lan, P.J. Li, J.M. Lin, L.Q. Fan, Application of microporous polyaniline counter electrode for dye-sensitized solar cells, Electrochemistry Communications 10 (2008) 1299–1302.
[7] S.G. Pawar, S.L. Patil, A.T. Mane, B.T. Raut, V.B. Patil, Growth, characterization and gas sensing properties of polyaniline thin films, Archives of Applied Science Research 1 (2) (2009) 109–114.
[8] S.R. Nalage, M.A. Chougule, Shashwati Sen, V.B. Patil, Fabrication and characterization of nickel oxide NO_2 sensor, Journal of Materials Science: Materials in Electronics 24 (2013) 368–375.
[9] S.T. Navale, S.R. Nalage, M.A. Chougule, S.A. Pawar, V.B. Patil, Novel process for synthesis of α-Fe_2O_3: microstructural and optoelectronic investigations, Journal of Materials Science: Materials in Electronics 24 (2013) 1422–1430.
[10] M.A. Chougule, S.G. Pawar, P.R. Godse, R.D. Sakhare, Shashwati Sen, V.B. Patil, Sol–gel derived Co_3O_4 thin films: effect of annealing on structural, morphological and optoelectronic properties, Journal of Materials Science: Materials in Electronics 23 (3) (2012) 772–778.
[11] D.M. Jundale, P.B. Joshi, Shashwati Sen, V.B. Patil, Nanocrystalline CuO thin films: synthesis, microstructural and optoelectronic properties, Journal of Materials Science: Materials in Electronics 23 (2012) 1492–1499.
[12] S.R. Nalage, M.A. Chougule, Shashwati Sen, P.B. Joshi, V.B. Patil, Sol gel synthesis of nickel oxide thin films and their characterization, Thin Solid Films 520 (2012) 4835–4840.
[13] S.G. Pawar, S.L. Patil, M.A. Chougule, V.B. Patil, Synthesis and characterization of nanocrystalline TiO_2 thin films, Journal of Materials Science: Materials in Electronics 22 (2011) 260–264.
[14] V.V. Chabukswar, S. Pethkar, A.A. Athawale, Acrylic acid doped polyaniline as an ammonia sensor, Sensorors and Actuatuators B: Chemical 77 (2001) 657–663.
[15] S.G. Pawar, S.L. Patil, M.A. Chougule, B.T. Raut, P.R. Godase, R.N. Mulik, et al., New method for fabrication of CSA doped PANi-TiO_2 thin-film ammonia sensor, IEEE Sensors Journal 11 (2011) 2980–2985.
[16] B.T. Raut, M.A. Chougule, A.A. Ghanwat, R.C. Pawar, C.S. Lee, V.B. Patil, Polyaniline-CdS nanocomposites: effect of camphor sulfonic acid doping on structural, microstructural, optical and electrical properties, Journal of Materials Science: Materials in Electronics 23 (2012) 2104–2109.
[17] S.L. Patil, S.G. Pawar, V.B. Patil, Polyaniline-ZnO nanocomposites: effect of camphor sulfonic acid doping on structural, morphological, optical and electrical transport properties, Soft Nanoscience Letters 2 (2012) 46–53.
[18] M.A. Chougule, G.D. Khuspe, Shashwati Sen, V.B. Patil, Polypyrrole-ZnO nanohybrids: effect of CSA doping on structure, morphology and optoelectronic properties, Applied Nanoscience (2013), http://dx.doi.org/10.1007/s13204-012-0149-x.
[19] M.A. Chougule, Shashwati Sen, V.B. Patil, Polypyrrole-ZnO hybrid sensor: effect of camphor sulfonic acid doping on physical and gas sensing properties, Synthetic Metals 162 (2012) 1598–1603.
[20] G.D. Khuspe, S.T. Navale, M.A. Chougule, V.B. Patil, Facile method of synthesis of Polyaniline-SnO_2 hybrid nanocomposite: Microstructural, optical and electrical transport properties, Synthetic metals 178 (2013) 1–9.
[21] G.D. Khuspe, S.T. Navale, D.K. Bandgar, R.D. Sakhare, M.A. Chougule, and V.B. Patil,SnO_2 nanoparticles-modified polyaniline films as highly selective, sensitive, reproducible and stable ammonia sensors, Journal of Electronic Materials Letters (2013), http://dx.doi.org/10.1007/s13391-013-3096-0.
[22] R.D. Sakhare, G.D. Khuspe, S.T. Navale, R.N. Mulik, M.A. Chougule, R.C. Pawar, C.S. Lee, Shashwati Sen, V.B. Patil, Nanocrystalline SnO_2 thin films: structural, morphological, electrical transport and optical studies, Journal of Alloys and Compounds 563 (2013) 300–306.
[23] G.D. Khuspe, R.D. Sakhare, S.T. Navale, M.A. Chougule, R.N. Mulik, R.C. Pawar, C.S. Lee, V.B. Patil, Nanostructured SnO_2 thin film for NO_2 gas sensing applications, Ceramic International 39 (2013) 8673–8679.
[24] S.G. Pawar, S.L. Patil, M.A. Chougule, B.T. Raut, V.B. Patil, Camphor sulfonic acid doped polyaniline–titanium dioxide nanocomposite: synthesis, structural, morphological and electrical properties, International Jounal of Polymeric Materials 60 (2011) 979–987.
[25] X.R. Zeng, T.M. Ko, Structure and properties of chemically reduced polyaniline, Polymer 39 (1998) 1187–1195.
[26] S. Palaniappan, B.H. Narayana, Composition and spectral studies of polyaniline salts, Polymers for Advanced Technologies 5 (1994) 225–230.
[27] S. Quillard, B. Corraze, M.I. Boyer, E. Fayad, G. Louarn, G. Froyer, Vibrational characterization of crystallized oligianiline: a model compound of polyaniline, Journal of Molecular Structure 596 (2001) 33–40.
[28] E.T. Kang, K.G. Neoh, K.L. Tan, Polyaniline: a polymer with many interesting intrinsic redox states, Progress in Polymer Science 23 (1998) 277–324.
[29] N. Colak, B. Sokmen, Doping of chemically synthesized polyaniline, Designed Monomers and Polymers 3 (2000) 181–189.
[30] H. Liu, X.B. Hu, J.Y. Wang, R.I. Boughton, Structure, conductivity, and thermo power of crystalline polyaniline synthesized by the ultrasonic irradiation polymerization method, Macromolecules 35 (2002) 9414–9419.
[31] Yuanchang Libo Sun, Zhaopin Shi, Bo He, Jiurong Li, Liu, synthesis and characterization of SnO_2/polyaniline nanocomposites by sol–gel technique and microemulsion polymerization, Synthetic Metals 162 (2012) 2183–2187.
[32] Lina Gang, Yingqiang Zhao, Xueliang Huang, Shurong Wang, Shoumin Zhang, Shihua Wu, Characterization and gas sensitivity study of polyaniline/SnO_2 hybrid material prepared by hydrothermal route, Sensors and Actuators B 120 (2007) 568–572.
[33] E. Kymakis, I. Alexandou, G.A.J. Amaratunga, Single-walled carbon nanotube-polymer composites: electrical, optical and structural investigation, Synthetic Metals (2002) 59–62.
[34] Y.P. Maminya, V.V. Davydenko, P. Pissis, E.V. Lebedev, Electrical and thermal conductivity of polymers filled with metal powders, European Polymer Journal 38 (2002) 1887.
[35] J.C. Huang, Carbon black filled conducting polymers and polymer blends, Advances in Polymer Technology 21 (4) (2002) 299–313.